

Effects of Land Cover Change on the Energy and Water Balance of the Mississippi River Basin

TRACY E. TWINE

Center for Sustainability and the Global Environment, Nelson Institute for Environmental Studies, and Department of Atmospheric and Oceanic Sciences, University of Wisconsin—Madison, Madison, Wisconsin

CHRISTOPHER J. KUCHARIK

Center for Sustainability and the Global Environment, Nelson Institute for Environmental Studies, University of Wisconsin—Madison, Madison, Wisconsin

JONATHAN A. FOLEY

Center for Sustainability and the Global Environment, Nelson Institute for Environmental Studies, and Department of Atmospheric and Oceanic Sciences, University of Wisconsin—Madison, Madison, Wisconsin

(Manuscript received 13 October 2003, in final form 20 February 2004)

ABSTRACT

The effects of land cover change on the energy and water balance of the Mississippi River basin are analyzed using the Integrated Biosphere Simulator (IBIS) model. Results of a simulated conversion from complete forest cover to crop cover over a single model grid cell show that annual average net radiation and evapotranspiration decrease, while total runoff increases. The opposite effects are found when complete grass cover is replaced with crop cover. Basinwide energy and water balance changes are then analyzed after simulated land cover change from potential vegetation to the current cover (natural vegetation and crops). In general, net radiation decreases over crops converted from forest and increases over crops converted from grasslands. Evapotranspiration rates decrease over summer crops (corn and soybean) converted from forest and increase over summer crops converted from grassland. The largest decreases ($\sim 0.75 \text{ mm day}^{-1}$; 20%) are found in summer over former forests, and the largest increases ($\sim 0.4 \text{ mm day}^{-1}$; 45%) are found in spring over former northern grasslands. Drainage rates increase over summer crops converted from savanna and forest and decrease over summer crops converted from grasslands. The largest increases ($\sim 0.6 \text{ mm day}^{-1}$; 45%) are found in winter over summer crops in former southern forests, and the largest decreases ($\sim 0.4 \text{ mm day}^{-1}$; 25%) are found in summer over summer crops grown in former northern grasslands. The simulated energy and water balance changes resulting from land cover change depend on season, crop type (winter, spring, or summer plantings) and management, and the type of natural vegetation that is removed.

1. Introduction

Through the conversion of forests and grasslands to croplands and pastures, humans have affected the exchange of energy, water, and carbon between the atmosphere and land surface. In order to face land and water resource challenges in the coming decades, we need to understand the relationships between land surface characteristics and energy, water, and nutrient cycles. Furthermore, we need to quantify how these relationships might change with changes in land cover, land management, and climate.

Incoming shortwave radiation drives the water cycle.

Even small changes in the surface albedo may significantly affect the timing and magnitude of evaporative losses to the atmosphere and, in turn, the amount of water that enters the soil and eventually reaches streams. While current satellite technology has made remote observations of land surface albedo possible, estimates of albedo changes and the resulting changes in radiative forcing from land cover change have produced a continuum of possible values (Myrhe and Myrhe 2003). Several studies (Hansen 1998; Betts 2001; Myrhe and Myrhe 2003) have concluded that land cover conversion from forests to croplands leads to decreases in annual average radiative forcing of the land surface.

Albedo changes are not the only way in which land cover changes affect the energy and water balance. Bosch and Hewlett (1982) reviewed 94 catchment experiments from around the world, of which 93 showed

Corresponding author address: Tracy E. Twine, SAGE, 1710 University Avenue, Madison, WI 53726.
E-mail: tetwine@wisc.edu

a significant increase in runoff after vegetation cover was decreased either through complete removal of vegetation or species replacement. Several modeling studies have related land cover change to potential changes in regional climate (Dickinson and Henderson-Sellers 1988; Chase et al. 1996; Copeland et al. 1996; Bonan 1997, 1999; Pielke et al. 1999), but only a few have examined the hydrologic response of large river basins to land cover change (Vorosmarty et al. 1989; Vorosmarty and Moore 1991; Costa and Foley 1997; Matheussen et al. 2000). Simulations have shown that replacing forest, woodland, and savanna with grassland over the Amazon River basin (Costa and Foley 1997) and deforesting the Columbia River basin either through species replacement or logging (Matheussen et al. 2000) lead to increased streamflow.

Much less is known about the hydrologic effects of replacing forests or grasslands with annual crops. Baron et al. (1998) used the Regional Hydro-Ecologic Simulation System (RHESSys) model to study the changes in evapotranspiration in the South Platte River basin after steppe vegetation was converted to rain-fed and irrigated agroecosystems. They found increases in evaporative losses to the atmosphere and in the length of the evaporative season (i.e., the length of time that evapotranspiration occurs from the land surface) after conversion to crops. These results suggest that changes in evaporative losses and runoff and streamflow may depend upon the exact form of land cover conversion.

Here we examine how the biophysical processes that occur with land cover change lead to shifts in the large-scale energy and water balance across the Mississippi River basin. We have adapted a global land surface/ecosystem model for use at a regional scale and have included algorithms that simulate the planting, phenology, and harvest of the major crop types grown within the Mississippi River basin. Using this model we examine how changes in land cover (from natural forests, savannas, and grasslands to various crop types) have affected the energy and water balance across the region.

In section 2, we describe how we have adapted a land surface/ecosystem model for use over the Mississippi River basin. In section 3, we analyze results of a single grid cell model simulation that shows how land cover change affects biophysical processes. We describe the model simulation over the entire basin in section 4 and analyze results from this simulation in section 5.

2. Methods: The regional IBIS model

We used the Integrated Biosphere Simulator (IBIS) land surface/ecosystem model (Foley et al. 1996; Kucharik et al. 2000) to evaluate the effects of land cover change on the energy and water balance in the Mississippi River basin. In particular, we used the model to evaluate land surface energy and water balance changes resulting from a conversion of potential vegetation (i.e., vegetation that could grow in an area without the influ-

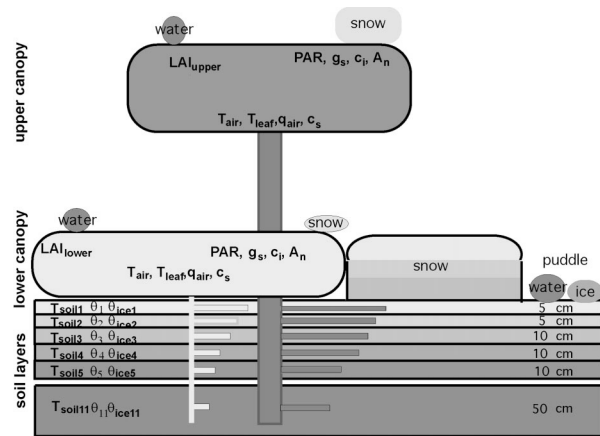


FIG. 1. IBIS grid cell showing the vegetation canopies, snow layers, soil layers, and the variables simulated at each time step. There are 11 soil layers extending from the surface to a depth of 2.5 m. PAR represents photosynthetically active radiation; g_s , stomatal conductance; c_i , CO_2 concentration in intercellular air spaces of leaf; A_n , net canopy photosynthesis; T_{air} , air temperature within canopy; T_{leaf} , leaf temperature; q_{air} , specific humidity of canopy air; C_s , CO_2 concentration at the leaf surface; $T_{\text{soil},x}$, soil temperature at layer x ; θ_s , soil moisture content at layer x ; $\theta_{\text{ice},x}$, ice content at layer x . Adapted from Kucharik et al. (2000).

ence of humans) to the current distribution of land cover that contains both natural vegetation (forests, savannas, and grasslands) and crops (mainly corn, soybeans, and wheat).

IBIS is a global-scale model that includes modules for vegetation canopy physics, soil physics and hydrology, vegetation phenology, and ecosystem biogeochemistry. Much of the land surface module structure has been borrowed from the land surface transfer scheme LSX (Thompson and Pollard 1995a; Thompson and Pollard 1995b). The global version of IBIS has been tested and validated against surface flux observations (Delire and Foley 1999), global compilations of ecosystem and hydrological data (Foley et al. 1996; Kucharik et al. 2000), hydrological data from the Amazon River basin (Costa and Foley 1997; Coe et al. 2002; Foley et al. 2002), and hydrological and ecosystem observations across the Mississippi River basin (Lenters et al. 2000; Kucharik et al. 2001; Donner et al. 2002; Donner 2003; Donner and Kucharik 2003). Results of the Lenters et al. (2000) study demonstrated that while hydrological processes are simulated reasonably well in IBIS, a regional version of IBIS adapted specifically for the continental United States should be developed in order to better capture land surface processes that are characteristic of the Mississippi River basin.

Each $0.5^\circ \times 0.5^\circ$ IBIS grid cell has the potential to represent two vegetation canopy levels: an upper-level forest canopy and a lower level of shrubs and C3 (cool) and C4 (warm) grasses. The model also includes 3 layers of snow and 11 soil layers extending to a depth of 2.5 m (Fig. 1). IBIS explicitly represents the leaf area index (LAI) of each canopy, the temperature of the soil (or

snow) surface and the vegetation canopies, as well as the temperature and humidity within the canopy air spaces. IBIS simulates the exchange of both solar and infrared radiation between the atmosphere, vegetation canopies, and the surface. The radiative properties (e.g., reflectivity, transmissivity) of canopies, soil, and snow are uniquely calculated and then related to the incoming radiation characteristics (e.g., fraction of diffuse and direct beam radiation and zenith angle). As a result, the surface albedo is a function of the vegetation cover, the soil type, and the incoming solar radiation.

The total amount of evapotranspiration from the land surface is treated as the sum of three water vapor fluxes: evaporation from both dry and wet soil surfaces, evaporation of water intercepted by vegetation canopies, and plant canopy transpiration. Evaporation rates are calculated using standard mass transfer equations relating the temperature of the surface, vapor pressure deficit, and conductance (Campbell and Norman 1998). Rates of transpiration depend on canopy conductance and are calculated independently for each plant functional type (PFT) within the canopy. Physiological processes are simulated with a mechanistic treatment of canopy photosynthesis (Farquhar et al. 1980; Farquhar and Sharkey 1982) and a semimechanistic model of stomatal conductance (Ball et al. 1987).

IBIS uses a multilayer formulation of soil to simulate the diurnal and seasonal variations of heat and moisture in the soil. At each 1-h time step, each layer is described in terms of soil temperature, volumetric water content, and ice content. The IBIS soil physics module uses Richard's equation to calculate the time rate of change of liquid soil moisture, and the vertical flux of water is modeled according to Darcy's law (Campbell and Norman 1998).

A more detailed description of the global version of IBIS containing additional module descriptions of vegetation competition, plant productivity, and below-ground cycling of carbon and nitrogen can be found in Kucharik et al. (2000).

We made two types of changes to the global version of IBIS in order to adapt it for use over the Mississippi River basin. First we improved the natural vegetation phenology algorithm and added modules that simulate the management (e.g., planting date, crop selection and rotation, and harvest date) and growth (carbon and nitrogen allocation, phenology) of crops. Then we integrated high-quality land cover, climate, and soils datasets as inputs to the model. Here we discuss changes to model algorithms. The new input datasets are described in section 4.

We improved the timing of plant bud burst and senescence, or phenology, by incorporating an algorithm developed by White et al. (1997) that is based on satellite and ground-level measurements of green vegetation. Previous versions of IBIS used phenology algorithms based on summations of growing degree-days that were calibrated to global-scale satellite observations

(Botta et al. 2000). Using the global version of IBIS (Kucharik et al. 2000), we found that bud burst at 13 grid cells within the Mississippi River basin occurred, on average, 35 days earlier, and senescence was delayed by 65 days, when values were compared with the measurements of White et al. (1997). The new algorithm improved the simulation of natural vegetation phenology by largely correcting the early and late biases through the use of empirical equations based on growing degree-days, precipitation accumulation, moisture stress within the vegetation, and root-zone temperature.

Previous versions of IBIS also allowed the total (green/living and brown/dormant) LAI of grasses to approach zero after senescence. However, real grass leaves generally remain on the stem throughout winter and turn from green to brown during senescence and remain this way during dormancy. In this version of the model, tree and shrub leaves of deciduous PFTs are allowed to die during winter so that LAI approaches zero, while grass leaves and stems remain standing but change from green to brown during senescence as they become physiologically dormant in the fall and from brown to green when growth begins in spring. The onset of the growing season is dependent on soil temperature. The C3 and C4 grasses have different temperature thresholds, and cool grasses must also reach a precipitation threshold before onset. Temperature and water stress thresholds control the offset of photosynthesis in fall.

The regional version of IBIS also contains additions that allow the simulation of the planting, phenology, and harvest of crops grown within the Mississippi River basin—specifically, corn, soybean, winter wheat, and spring wheat (Fig. 2). The crop algorithms are based on the differences in C3 and C4 physiology and crop phenology that responds to management options (e.g., irrigation, fertilizer application, planting date) and environmental stresses (water and nitrogen stresses and climate). IBIS uses summations of growing degree-days to determine when crops have reached one of three growing phases: leaf emergence, grain fill, and harvest, in a manner similar to the Crop Environment Resource Synthesis (CERES-Maize) and Erosion/Productivity Impact Calculator (EPIC) crop models (Jones and Kiniry 1986; Sharpley and Williams 1990). Algorithms simulate crop yield, dry matter production, harvest index, daily LAI, root growth and turnover, total plant nitrogen uptake, net nitrogen mineralization, plant tissue carbon and nitrogen, soil carbon and nitrogen, soil carbon dioxide flux, and evapotranspiration (Kucharik 2003; Kucharik and Brye 2003).

The IBIS regional model has been used to study carbon sequestration (Kucharik et al. 2001), the response of nitrate leaching losses and corn yield to varied nitrogen fertilizer management (Kucharik and Brye 2003), nitrogen leaching (Donner and Kucharik 2003), and mean crop yield and variability in the Mississippi River basin (Kucharik 2003). IBIS has been validated at a research station in Wisconsin with 6 yr of measurements

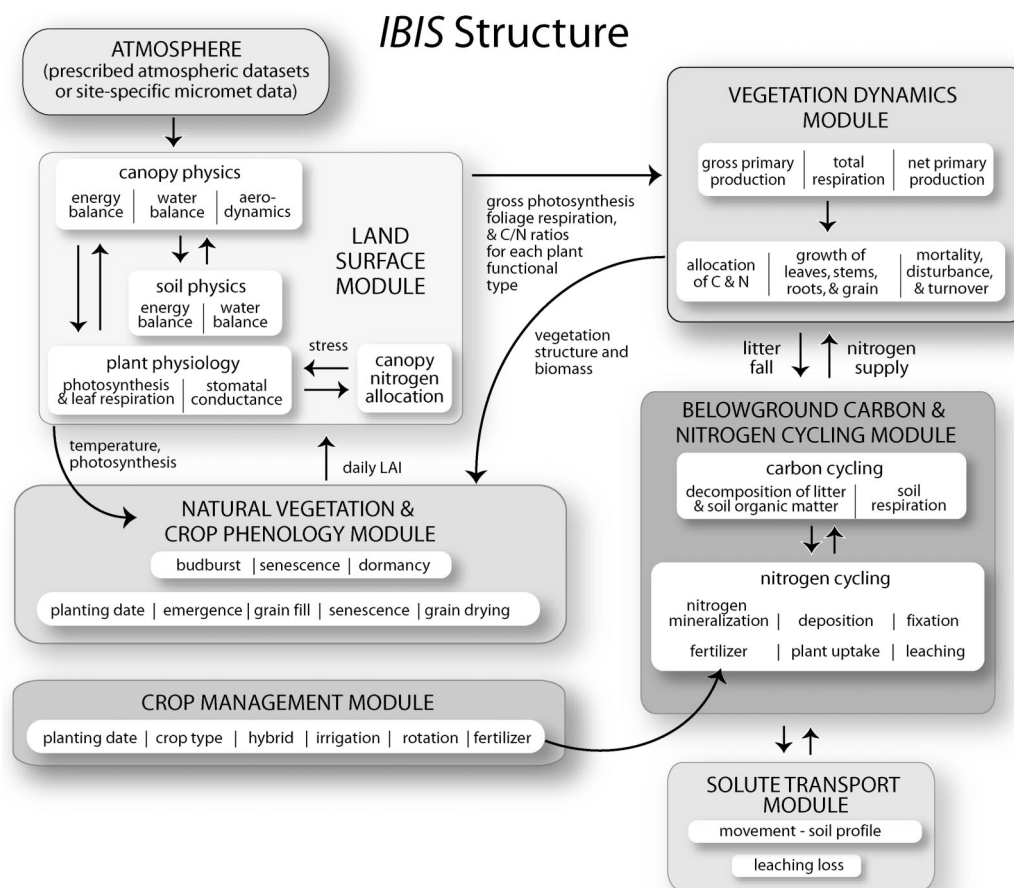


FIG. 2. Schematic of the regional IBIS model that includes modules for land surface physics, vegetation phenology and dynamics, below-ground biogeochemistry, crop management, and solute transport. Adapted from Kucharik (2003).

of corn grain yield, harvest index, plant nitrogen uptake, residue carbon to nitrogen ratio, LAI development, net nitrogen mineralization, extractable soil nitrate, annual nitrate leaching, fall soil inorganic nitrogen storage, flow-weighted mean annual nitrate concentration in leachate solutions, and annual drainage (Kucharik and Brye 2003).

3. Changes in land surface energy and water balance: A single grid cell

In order to better understand the physics behind the energy and water balance changes in our basinwide simulation of land cover change, we first ran the model several times, each time with a different type of vegetation cover, over a single grid cell in western Wisconsin (43.75°N, 90.75°W). A similar hourly climate forcing, including timing and amount of precipitation events, was used in all runs with a 1-h time step. The same inputs and spinup period were used for this suite of simulations as in the basinwide simulations, as explained in section 4. A 20-yr run was selected to allow a sufficient length of time for annual averages, and the

particular period (1961–80) was chosen to be within the 38-yr basinwide simulation (1958–95).

Since the main potential vegetation types of the Mississippi River basin are grassland (42% of the basin, by area) and temperate deciduous forest (23% of the basin), we ran the model assuming the grid cell was completely covered (100%) with deciduous forest and then again with grassland. We ran the model three more times assuming a complete cover of winter crops (winter wheat), spring crops (spring wheat), and then summer crops (corn and soybeans) to determine how the specific crop type might affect net radiation, evapotranspiration, and total runoff throughout the year. Winter wheat is planted in fall and harvested in late spring, spring wheat is planted in spring and harvested in midsummer, and summer crops are planted in spring and harvested in early fall. These changes in growing season, along with changes in land surface characteristics, contribute to changes in the energy and water balance after conversion. Examples of surface characteristics that change with land cover conversion are given in Table 1.

We computed 20-yr monthly averages of the hourly simulated energy and water balance variables for the

TABLE 1. Surface parameters that change upon conversion from forest or grassland to crop cover. Many of the changes in these parameters are caused by differences in the growing seasons of the vegetation types. For example, at any particular time, the roughness height of grasses and crops may be different because of the difference in growing seasons (and LAI), even if the maximum value of canopy height of both grasses and crops is equal. Physiological and phenological changes in vegetation occur with conversion, but there is no change to soil texture and soil hydraulic properties.

	Surface albedo (vegetation + soil)	Leaf optical properties	Max canopy height	LAI	Roughness height	Rooting distribution
Forest to crops	Increases	Near-infrared (NIR) re- flectance and visible and NIR transmit- tance increases	Decreases	Decreases	Varies with season	Becomes more shallow
Grassland to crops	Varies with season	Grass leaves can be green or brown		Varies with season	Varies with season	

five vegetation types. Only results from the corn cover simulation are given for the summer crop analysis because the soybean cover simulation results were similar. The summer crop cover results are assumed to be representative of both corn and soybean.

a. Deciduous forest conversion to crops

Figures 3a, 3c, and 3e show that when the forest-covered grid cell is completely deforested and replaced with 100% crop cover, annual average net radiation de-

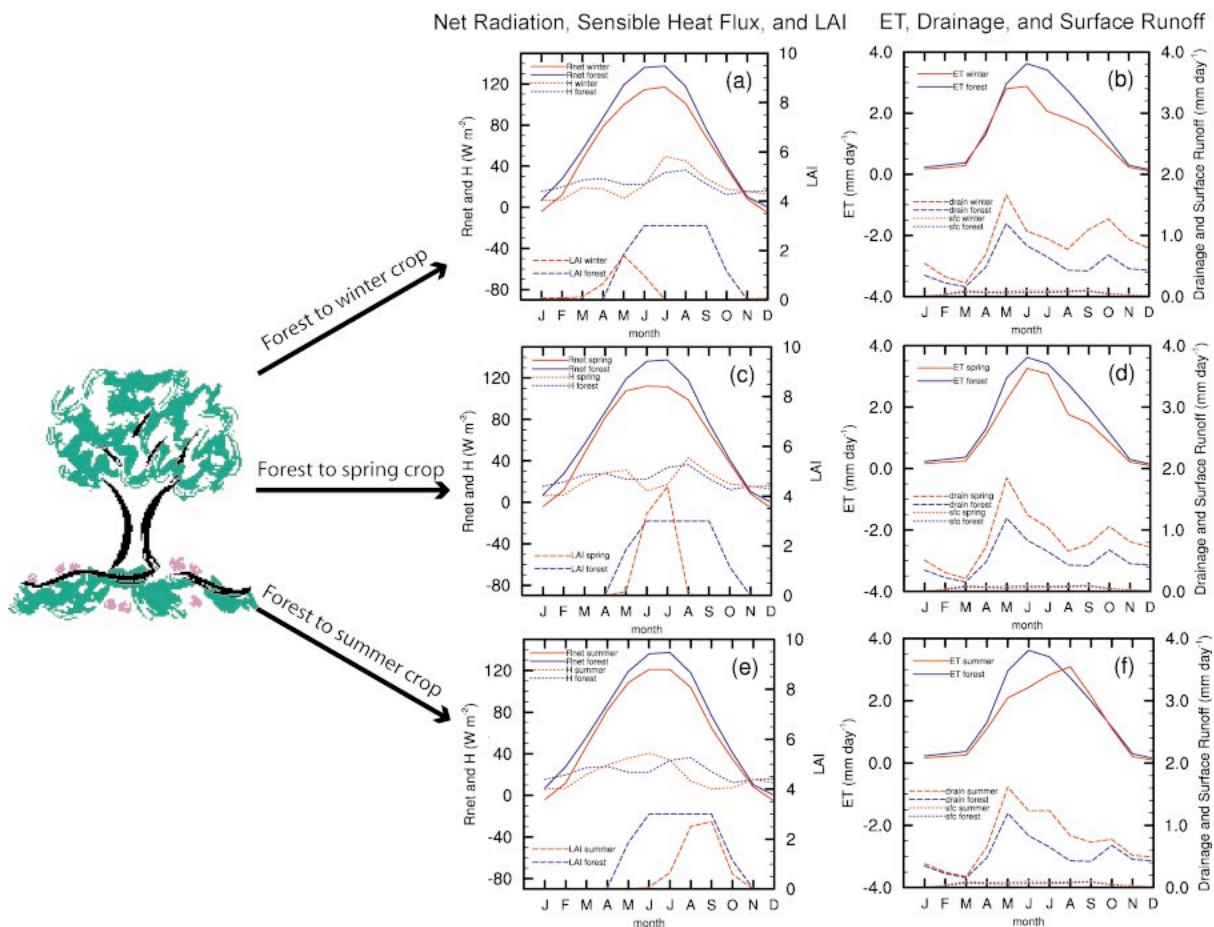


FIG. 3. IBIS-simulated single grid cell values of (a) net radiation ($W m^{-2}$), sensible heat flux ($W m^{-2}$), and LAI and (b) ET ($mm day^{-1}$), surface runoff ($mm day^{-1}$), and subsurface drainage ($mm day^{-1}$) for 100% forest cover and 100% winter crop cover. (c) As in (a), and (d) as in (b) for 100% forest cover and 100% spring crop cover. (e) As in (a), and (f) as in (b) for 100% forest cover and 100% summer crop cover.

TABLE 2. Annual average changes to net radiation, ET, surface runoff, and drainage after 100% land conversion from two potential vegetation covers (deciduous forest and grassland) to three crop covers (winter crop, spring crop, and summer crop) simulated over one 0.5° grid cell.

Potential vegetation	Crop cover	Changes to net radiation (W m ⁻²)	Changes to ET (mm day ⁻¹)	Changes to surface runoff (mm day ⁻¹)	Changes to drainage (mm day ⁻¹)
Deciduous forest	Winter	↓ 12 (17%)	↓ 128 (23%)	↑ 5 (26%)	↑ 122 (63%)
Deciduous forest	Spring	↓ 12 (17%)	↓ 116 (20%)	↑ 5 (26%)	↑ 110 (57%)
Deciduous forest	Summer	↓ 10 (14%)	↓ 85 (15%)	↑ 5 (26%)	↑ 79 (41%)
Grassland	Winter	↑ 9 (19%)	↑ 30 (7%)	↓ 1 (4%)	↓ 29 (8%)
Grassland	Spring	↑ 9 (19%)	↑ 42 (10%)	↓ 1 (4%)	↓ 41 (12%)
Grassland	Summer	↑ 11 (23%)	↑ 73 (17%)	↓ 1 (4%)	↓ 72 (20%)

creases by about 10 W m⁻² (15%), regardless of crop type (Table 2). Since all simulations were driven with the same hourly climate data (air temperature, precipitation, cloud cover), all changes in net radiation result solely from changes in surface albedo and outgoing infrared (IR) radiation fluxes. The largest net radiation differences occur in winter (40%) and summer (10%) when albedo differences are greatest. Albedo differences are large because of snow effects in winter and because of differences in leaf optical properties and LAI between the natural vegetation and crops in summer. Net radiation is less in winter because the albedo of the snow-covered barren crop fields is greater than that of the bare trunks and branches of deciduous trees (Hansen 1998; Betts 2001). During the crop-growing season, net radiation over croplands is less because the decrease in LAI with conversion causes an increase in albedo as more soil is exposed, while just before and after the growing season the net radiation is less because IR fluxes from bare crop fields are greater.

Seasonal changes in latent heat flux (LE) and sensible heat flux (H) are dependent on crop type, but all simulations show that crop H is less during the particular crop-growing season but greater when crop fields are bare (Figs. 3a, 3c, and 3e). For example, during May after a conversion to winter wheat cover, the winter wheat has reached its peak growth, and LE (not shown) is similar to forest LE. Because the net radiation is less over winter wheat cover from increased albedo, and soil heat flux changes are small, winter wheat H is less. Soil heat flux and LE are not plotted, but patterns of LE change after conversion can be seen in the evapotranspiration (ET) plots shown in Figs. 3b, 3d, and 3f.

While little data are available to validate the sensitivity of the simulated energy balance terms to vegetation change, the validation of IBIS with measurements from several field experiments has shown that IBIS can successfully simulate the surface energy balance over different vegetation types. Delire and Foley (1999) tested IBIS with soil temperature, soil moisture, and energy flux data over a soybean crop in France [Hydrological Atmospheric Pilot Experiment—Modélisation du Bilan Hydrique (HAPEX-MOBILHY), 1986], a meadow in the Netherlands (Cabauw, 1987), a grassland in Russia (Valday watershed study area and Usadievskiy grassland site, 1966–83; information available online at [\[climate.envsci.rutgers.edu/soil_moisture/valdai.html\]\(http://climate.envsci.rutgers.edu/soil_moisture/valdai.html\)\), a prairie in Kansas \[First International Satellite Land Surface Climatology Project \(ISLSCP\) Field Experiment \(FIFE\), site 16, 1987–89\], and a tropical forest in Brazil \[Anglo-Brazilian Amazonian Climate Observation Study \(ABRACOS\), Reserva Jaru, 1992–93\]. A comparison of IBIS results with 37 days of 30-min observations over the soybean crop gave rms errors of 21 W m⁻² for net radiation \(maximum values were about 700 W m⁻²\), 42 W m⁻² for \$H\$, 72 W m⁻² for LE, and 14 W m⁻² for soil heat flux.](http://</p>
</div>
<div data-bbox=)

Evapotranspiration fluxes from crops and forest depend on the active photosynthetic period of the particular vegetation type (Figs. 3b, 3d, and 3f). In general, annual crop ET is less than or equal to forest ET; however, instantaneous crop ET fluxes can be greater than forest fluxes, especially from summer crops (Fig. 3f). Since this chosen grid cell received the same hourly climate forcing for all simulations, the decrease in annual ET with crops must be compensated by an increase in total runoff in order to conserve water. Total runoff in IBIS is simulated as

$$\text{Trun} = P - \text{ET} - \text{storage}, \quad (1)$$

where Trun is total runoff (the sum of surface runoff and subsurface drainage), P is precipitation, ET is evapotranspiration, and storage represents temporary reservoirs of water such as snow stored at the surface or soil moisture within the soil column. Storage is negligible at the annual time scale. Figures 3b, 3d, and 3f show that there is little to no change in the already low amount of monthly surface runoff; therefore, the decrease in crop ET results in an increase in subsurface drainage for most months. Observations of the partitioning between surface runoff and subsurface drainage after land cover change at the regional scale are not available to validate these results. Although evidence suggests that precipitation may change the soil surface structure in a manner that acts to increase surface runoff (J. Norman 2004, personal communication), IBIS does not simulate soil structure at any depth, and it is unclear how these small-scale effects would influence regional-scale average values of total runoff.

Decreased evaporation of canopy-intercepted water and transpiration after conversion contribute to increased subsurface drainage rates for most of the year

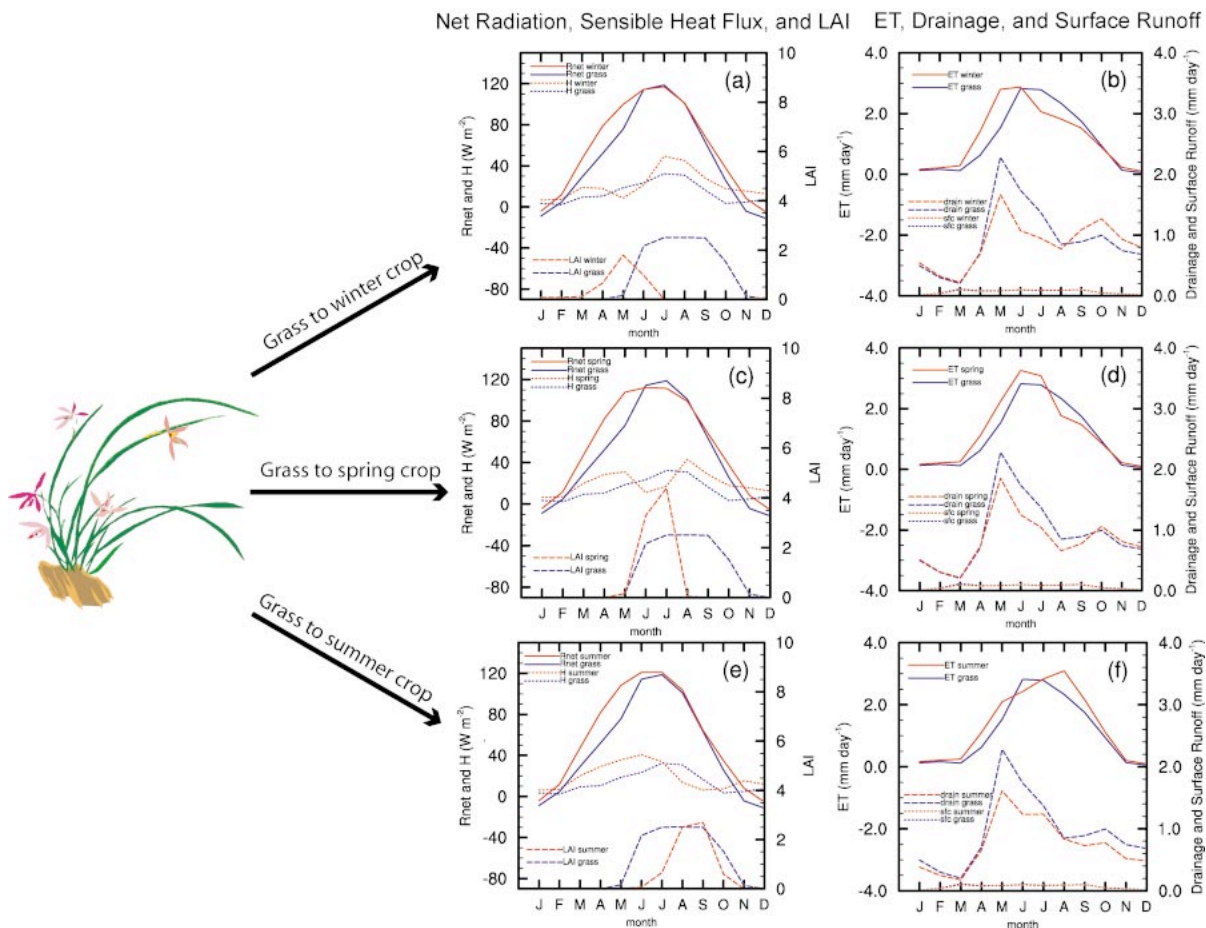


FIG. 4. As in Fig. 3 for a conversion from grassland to separate crop-type covers.

beginning with snowmelt in April (Figs. 3b, 3d, and 3f). The peak in drainage during fall is largest for winter crop cover because it is harvested earliest and the bare soil has all summer to infiltrate water. The summer crop drainage peak during fall is similar to that of the forest because summer crops are still transpiring in late summer and early fall.

On an annual basis, ET decreases by 23% (128 mm yr⁻¹) with a planted winter crop cover, by 20% (116 mm yr⁻¹) with spring crop cover, and by 15% (85 mm yr⁻¹) with summer crop cover. Annual drainage rates increase by 63% (122 mm yr⁻¹) with winter crop cover, by 57% (110 mm yr⁻¹) with spring crop cover, and by 41% (79 mm yr⁻¹) with summer crop cover (Table 2).

b. Grassland conversion to crops

The same grid cell in western Wisconsin was then subjected to land cover change from grassland to the three seasonal crop types. Unlike the forest conversion analysis, the differences in net radiation resulting from albedo change now depend on both LAI and leaf color

(whether grasses are growing or dormant). The LAI for grasses plotted in Figs. 4a, 4c, and 4e represents the green (or photosynthetically active) leaves. LAI values of zero imply that leaves are brown and are not photosynthetically active. IBIS climate-based thresholds allow only C3 grasses to grow within this grid cell.

Figures 3a, 3c, and 3e and Figs. 4a, 4c, and 4e show that, at this particular location, net radiation values of grasses are lower than those of trees, and crop net radiation values are mainly greater than or equal to those of grasses. The largest differences in net radiation occur in spring (~50%) when the crop albedo is less than the dormant (brown) grass albedo (Figs. 4a, 4c, and 4e). The difference in albedo results from different leaf optical properties between green and brown leaves. Green grass and crop leaves in IBIS have a visible leaf reflectance of 0.10 and a near-infrared reflectance of 0.58, while brown grass leaves have a visible leaf reflectance of 0.36 and a near-infrared reflectance of 0.58. Crop net radiation values become similar to those of grasses by June as the grassland begins its growing season, although the later date of leaf emergence of summer crops allows the net radiation to be slightly greater than grass-

es during the early summer when summer crop LAI is approximately 50% of maximum late-season values (Fig. 4e). Annual average net radiation values increase by about 10 W m^{-2} , or 22% after conversion (Table 2).

Crop H is lower during the crop-growing season, as the incoming radiation is used for transpiration, but is greater in spring when there is more net radiation than is used in evaporation from bare crop fields, and in fall (after the growing season) when crop net radiation is similar to grass net radiation but evaporation from harvested crop fields is less than grass transpiration (Figs. 4a, 4c, and 4e).

There is a distinct seasonal difference between peak ET rates of the grasses and crops, with an overall increase in annual ET after conversion to cropland (Table 2). Spring ET rates rise from minimal winter values as winter crops begin to transpire and as soil evaporation begins over bare spring and summer crop fields (Figs. 4b, 4d, and 4f). Dormant grass cover keeps grass ET rates lower at this time. Crop ET rates are less over winter and spring crop cover later in summer after harvest. However, because summer crops reach physiological maturity in late summer to early fall, summer crop ET rates are greater than grasses at this time. Annually, winter crop ET increases by about 7% (30 mm yr^{-1}), spring wheat ET by about 10% (42 mm yr^{-1}), and summer crop ET by about 17% (73 mm yr^{-1}) after conversion (Table 2).

The greater crop ET rates in spring contribute to a decrease in spring drainage for all crop types with negligible changes to surface runoff (Figs. 4b, 4d, and 4f). Fall drainage rate changes are dependent on crop type. The bare winter crop fields in summer cause high infiltration of summer precipitation that results in an increase in fall drainage after conversion (Fig. 4b). The later maturity of summer crops causes summer crop drainage to be lower than grasses in fall since transpiration rates are high through late summer (Fig. 4f). Fall drainage rates of spring crops are similar to those of grasses (Fig. 4d). A conversion of grassland to crops causes a decrease in annual average drainage of 8% (29 mm yr^{-1}) for winter crops, 12% (41 mm yr^{-1}) for spring crops, and 20% (72 mm yr^{-1}) for summer crops (Table 2).

We cannot validate these particular results because of a lack of observations of the effects of a complete replacement of natural vegetation with various crop types under similar climate conditions. While the IBIS model has compared favorably to point location observations of energy and carbon fluxes and soil temperature and moisture values over a variety of vegetation types, we do not know how sensitive the IBIS results are to changes in vegetation characteristics such as LAI and to model structure. The spring soil surface evaporation fluxes over crop fields appear to be too large and the ET fluxes from grasslands may be too small because IBIS does not simulate a residue layer that can contribute 20–30

mm of water to observed ET fluxes (J. Norman 2004, personal communication).

The largest decrease in drainage does not come from a conversion to the crop type with the largest LAI or with a growing season concurrent with maximum incoming solar radiation, but from a conversion to summer crops—the crop type that has the longest “evaporative season” (length of time that evapotranspiration occurs from the land surface). Although summer crops have the largest impact in the grassland analysis, they had the least impact in the forest analysis where there was no significant change to the length of the evaporative season. Our analysis shows that this is not because of physiological differences among crops but because of the difference in crop evaporative seasons. As a result, we find that the actual crop management regime (initial land cover, crop type, planting dates, harvesting dates, and residue management) is extremely important in these studies.

4. Modeling changes across the basin

We performed two IBIS simulations to assess the effect of land cover change on the energy and water balance of the Mississippi River basin (29° – 50° N, 115° – 78° W). For the first simulation, we used a potential vegetation land cover map, and for the second simulation we used a 1992 crop/natural land cover (or “current cover”) map. In order to isolate effects resulting solely from land cover change, we forced both simulations with the same hourly climate dataset and did not simulate any irrigation. IBIS was run at a 0.5° grid cell spatial resolution with an hourly time step for the period 1958–95 after a spinup of 100 yr that allowed the biogeochemistry calculations of the model to nearly reach equilibrium. The effect of land cover change on the energy and water balance was evaluated by analyzing the difference in model results between the current cover simulation and the potential vegetation cover simulation; differences were evaluated using the Student’s t test at the 90% significance level.

Here we describe the input datasets used to drive IBIS.

a. Climate and soils

We synthesized hourly weather and climate information from a combination of monthly climatic observations, daily reanalyzed meteorological data, and an hourly weather generator. We first used observed monthly values of air temperature, precipitation, vapor pressure, and cloud fraction from 1901 to 1995 along with 1961–90 climatological mean values of monthly wind speed, diurnal temperature range, and number of wet days per month as given by the University of East Anglia Climate Research Unit’s CRU05 climate dataset (New et al. 1999). In order to capture the transient, day-to-day phenomena of storm systems characteristic of the

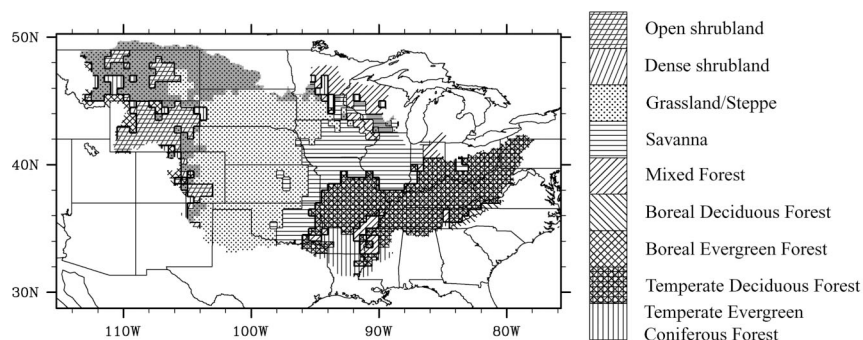


FIG. 5. Potential vegetation cover of the Mississippi River basin. The gray areas represent grasslands and savannas that are dominated by C3 grasses. Nonshaded grassland and savanna areas are dominated by mixtures of C4 and C3 grasses.

continental United States and to attempt to simulate spatial patterns of weather events, we combined the monthly CRU05 data with daily anomalies of temperature, precipitation, specific humidity, and cloud fraction from the National Centers for Environmental Prediction–National Center for Atmospheric Research (NCEP–NCAR) meteorological reanalysis dataset (Kalnay et al. 1996) to produce a daily value at each grid cell. The monthly average values of these daily values were forced to equal the monthly CRU05 values. Finally, hourly variations in climatic variables were simulated through the use of a simple statistical weather generator (Richardson 1981; Richardson and Wright 1984; Geng et al. 1985) that was forced with the previously determined daily value of each variable. The use of the weather generator ensured that precipitation fell as discrete events and not as constant drizzle throughout the day.

IBIS uses soil texture information to determine soil hydraulic properties for each soil layer (Rawls et al. 1992; Campbell and Norman 1998). We used soil texture input from the coterminous United States (CONUS) dataset (Miller and White 1998) by aggregating the original $1 \text{ km} \times 1 \text{ km}$ data to 0.5° resolution. We assigned the dominant 1-km resolution soil texture profile contained within each 0.5° grid cell to the value of the IBIS grid cell.

b. Vegetation cover

Our simulations used two land cover datasets. The first was a potential vegetation cover, that is, vegetation that could grow within the basin without human influence (Ramankutty and Foley 1998). This dataset was derived from the International Geosphere Biosphere Programme's 1-km DISCover land cover dataset (Loveland and Belward 1997) and historical vegetation maps of natural ecosystem extents. These data were projected onto an 8-km grid. Figure 5 shows that the main potential vegetation types of the Mississippi River basin are grassland, temperate deciduous forest, and temperate savanna—a combination of trees and grasses. Grassland can be found mainly in the western portion of the basin,

while savanna covers most of what is now the “corn-belt region,” and deciduous forest is found mainly in the eastern and southern portions of the basin.

The second land cover dataset consisted of 1992 maps of the fraction cover of corn, soybean, spring wheat, and winter wheat, compiled by Donner (2003), superimposed onto the potential vegetation cover map of Ramankutty and Foley (1998). The 8-km resolution crop cover maps (Fig. 6) were created by combining 1992 county-level U.S. agricultural inventory data for individual crops with the fractional cropland data of Ramankutty and Foley (1999). We assumed that each 8-km grid cell in our analysis was made up of some portion of crop cover and some portion of natural vegetation so that the sum of the fraction cover values of all crop types and natural vegetation was equal to 100%. We assumed that the natural vegetation cover of each grid cell was equal to the potential vegetation cover. About 20% of the potential grassland area is now cropland and about 15% of the potential deciduous forest is now cropland, while potential savanna has lost 44% of its area to cropland, mainly corn and soybean (Donner et al. 2002). According to the 1992 statistics, 8.4% of the total land area of the Mississippi River basin is covered by corn, 6.5% is covered by soybean, 4.7% is covered by winter wheat, and 1.1% is covered by spring wheat.

We ran IBIS once with the potential vegetation map and four more times for each crop type. We then used the 8-km fraction cover crop maps to weight the IBIS output according to the fraction cover of potential vegetation and individual crop type contained in each 8-km grid cell to create the output dataset for the “current cover” simulation.

5. Changes in the basinwide energy and water balance

In this section, we discuss how land cover change affects the simulated energy and water balance of the Mississippi River basin.

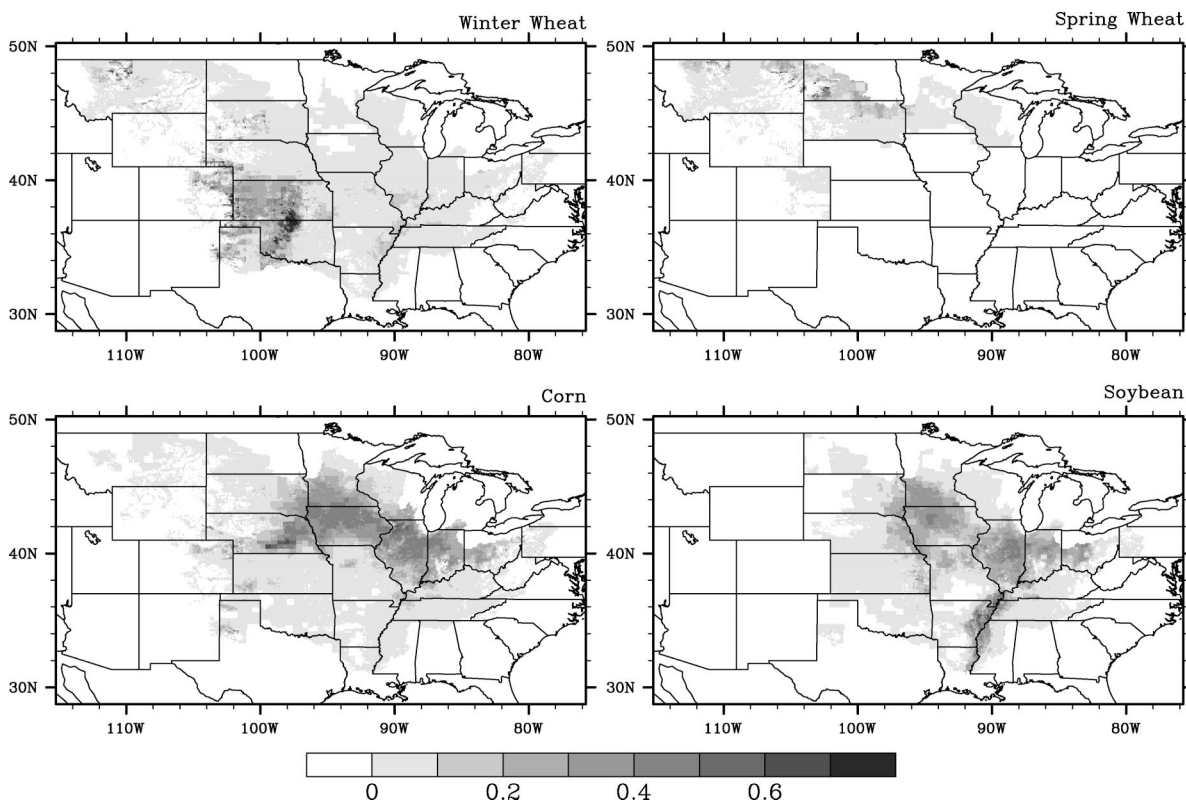


FIG. 6. Fraction cover of winter wheat, spring wheat, corn, and soybean as compiled by Donner (2003) from 1992 county-level census data and satellite information of crop cover.

a. Energy balance

In general, net radiation decreases in areas where forest has been converted to crops and increases where grassland has been converted to crops (Fig. 7), which is in agreement with the single grid cell results shown in Figures 3a, 3c, and 3e and Figs. 4a, 4c, and 4e. Winter net radiation values increase over former grasslands and savanna as the bare crop field albedo is lower than that of the dormant grasses. Even with some northern snow cover, the bare soil is darker than the dormant grass cover. The largest increases ($\sim 15 \text{ W m}^{-2}$; 145%) are found over winter crop fields in Oklahoma where the winter wheat is beginning its growth near the end of the fall season and the albedo of the green leaves is lower than that of the dormant grasses. Net radiation over former conifer and mixed forests of Minnesota and Indiana decreases as the bare (and snow-covered) crop field albedo is greater than the albedo of dark green needles (Hansen 1998; Betts 2001).

Differences in spring net radiation are largest over former grasslands ($\sim 25 \text{ W m}^{-2}$; 45%) and savanna ($\sim 15 \text{ W m}^{-2}$; 20%) (cf. Fig. 7 and Figs. 4a, 4c, and 4e). Snowmelt in northern areas causes the bare spring and summer crop field albedo to be lower than that of the former dormant grasses, and this effect continues through summer over summer crop fields even after the grass-growing season begins because summer crops are

the only type of crop where fields are relatively bare throughout the entire summer season. The net radiation decreases over winter crop fields as the crop has been harvested and outgoing IR fluxes from the bare fields are large.

The largest decreases of the year occur in summer over former savanna ($\sim 6 \text{ W m}^{-2}$; 5%) and forest (up to 15 W m^{-2} ; 10%) as crop albedo is greater than that of trees and outgoing IR fluxes over bare summer crop fields near the beginning of the summer season are larger. This decrease in net radiation results in a decrease in LE (not shown) as soil evaporation from bare crop fields and crop transpiration rates are less than transpiration from trees. There is also a decrease in H (not shown) over former conifer and mixed forests. Coniferous trees have lower transpiration rates than deciduous trees and greater sensible heat fluxes for the same amount of net radiation; therefore, a conversion from conifer or mixed forests to crops causes significant decreases in sensible heat fluxes.

Annually, the largest changes in net radiation ($\sim 13 \text{ W m}^{-2}$; 30%) are found where grasslands have been converted to winter and summer crops since these areas show the most consistent patterns of change throughout the seasonal averages. Small increases are found where savanna has been converted to summer crop ($\sim 5 \text{ W m}^{-2}$; 8%) and small decreases are found where forest

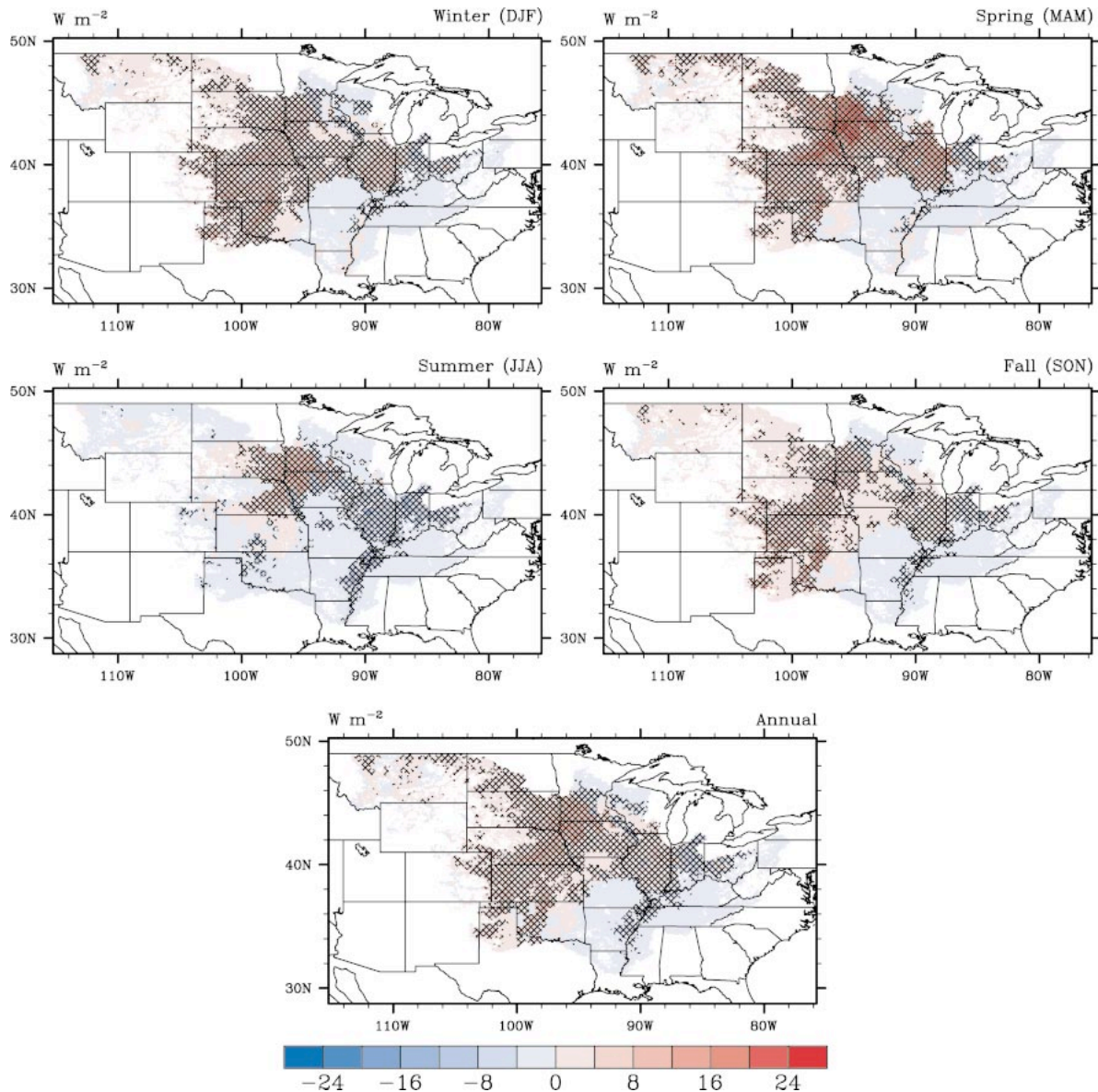


FIG. 7. Changes in seasonal and annual net radiation ($W m^{-2}$) between simulations (current cover – potential vegetation cover) for 1958–95. Differences significant at the 90% level are hatched.

has been converted to summer crops ($\sim 5 W m^{-2}$; 7%). The grasses of the former savanna seem to dominate the changes in net radiation throughout the year except during summer when the large LAI of trees lowers the albedo and dominates the overall signal.

b. Water balance

In our single grid cell analysis, a conversion of deciduous forest to summer crops led to a decrease in ET, while a conversion of grassland to crops led to an increase in the length of the evaporative season for all crops, particularly summer crops (Figs. 3 and 4). These phenomena are also evident in Fig. 8 as ET decreases

in all seasons when summer crops replace forest and ET increases in all seasons when summer crops replace grasslands. Evapotranspiration increases during three seasons when spring and winter crops replace grasslands.

There are significant, albeit small, increases in winter ET rates when crops replace grasslands. The largest changes ($\sim 0.25 mm day^{-1}$; 70%) are found over areas with the largest fraction cover of crop fields where unfrozen bare soil allows increased soil water evaporation. Significant decreases occur over former conifer and mixed forest in northeastern Iowa and from southern Michigan down through Indiana where there is much less evaporation of canopy-intercepted water.

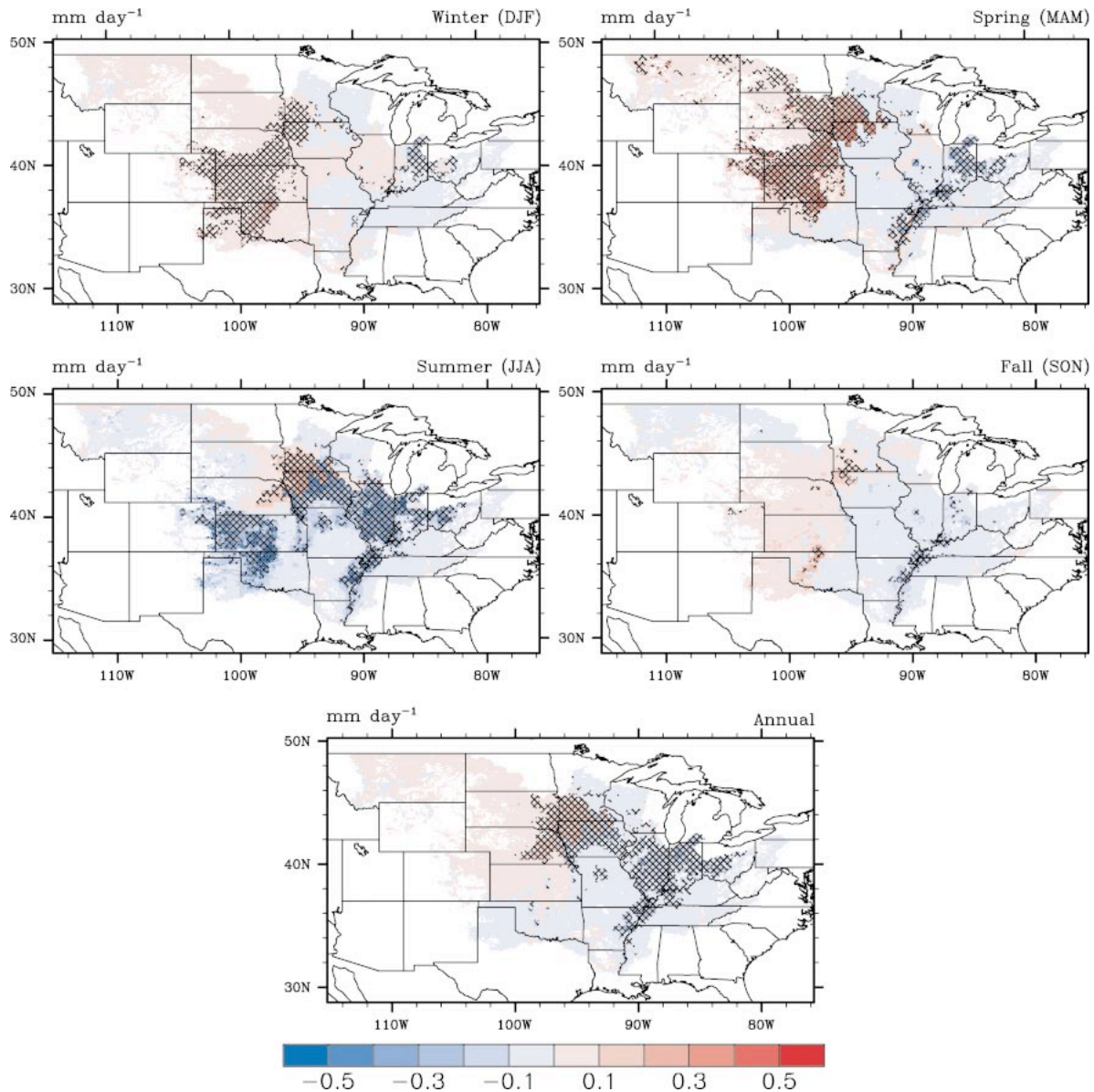


FIG. 8. Changes in seasonal and annual ET (mm day^{-1}) between simulations (current cover - potential vegetation cover) for 1958-95. Differences significant at the 90% level are hatched.

Spring ET rates are greater over areas of former grassland ($\sim 0.4 \text{ mm day}^{-1}$; 45%), where soil evaporation rates from bare spring and summer crop fields and transpiration rates from winter crop fields are greater than evaporation rates from the dormant grass cover (Fig. 8 and Figs. 4b, 4d, and 4f). Evapotranspiration rates decrease over most areas of former savanna and forest ($\sim 0.3 \text{ mm day}^{-1}$; 10%) where soil evaporation rates from bare crop fields are less than the transpiration from trees (Figs. 8 and 3f). Even though the grasses of the former savanna dominate the net radiation changes in spring, savanna trees account for the increase in ET with their high transpiration rates, although this change is not significant at 90%.

Although summer transpiration rates from summer crop fields in former grassland regions are greater (see Fig. 4f), summer is the season of largest decrease in ET in all other regions of the basin that have undergone land cover change (Fig. 8). Summer soil evaporation rates over the bare winter crop fields are lower than the transpiration rates of the former grassland ($\sim 0.75 \text{ mm day}^{-1}$; 20%), but very little changes are found over the growing spring wheat. Figures 3 and 4 show that summer transpiration rates of summer crops are less than those of trees but greater than those of grasses. Because ET rates over former savanna are lower, the trees of the savanna must dominate the ET signal in summer as well as in spring.

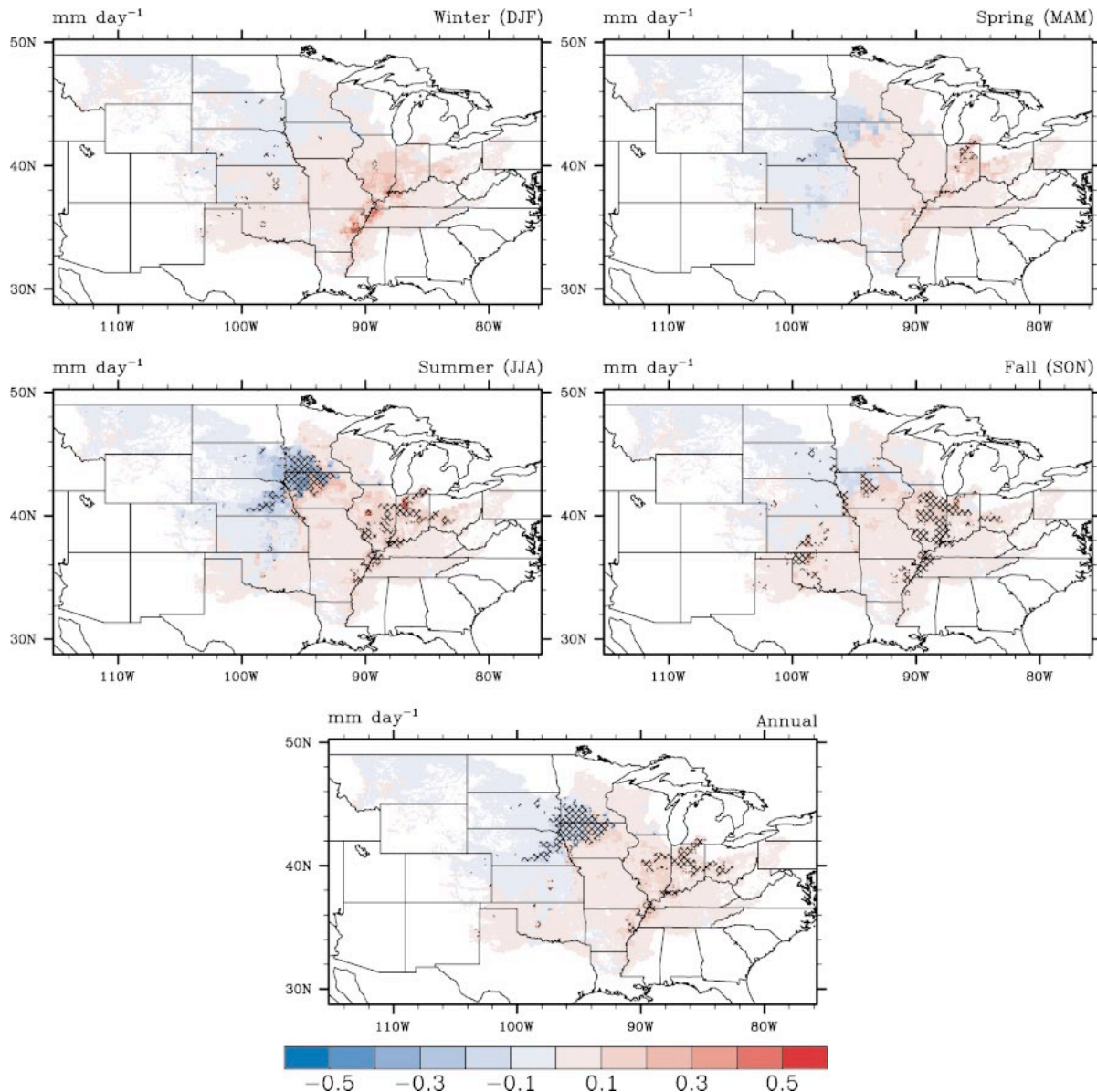


FIG. 9. Changes in seasonal and annual total runoff (mm day^{-1}) between simulations (current cover - potential vegetation cover) for 1958-95. Differences significant at the 90% level are hatched.

Evapotranspiration differences diminish in fall as summer crops reach physiological maturity. Now the ET rates are greater over areas of winter crops as soil evaporation from bare crop fields is greater than transpiration from senescing grasses. Several areas of significant decrease in ET can still be found along the lower Mississippi where there are large fraction cover values of soybeans, which tend to have a slightly longer growing season than crops grown to the north.

There are no statistically significant areas of change in annual average ET rates throughout the basin, although Fig. 8 shows decreases of $\sim 0.2 \text{ mm day}^{-1}$ (73 mm yr^{-1} , or 10%) over areas of former forest and savanna that have been converted to summer crops and

grassland that has been converted to winter crops, and increases of $\sim 0.2 \text{ mm day}^{-1}$ (73 mm yr^{-1} , or 15%) over areas of former grassland that have been converted to summer crops. There are negligible changes found over the region of spring crop cover in the northern Great Plains.

Because the amount and timing of precipitation in each grid cell is the same for both simulations, the total amount of water lost through evapotranspiration and total runoff is constant, but the partitioning between these two forms of water loss may change between simulations. Figures 8 and 9 show that increases (decreases) of ET are offset by decreases (increases) in total runoff. Winter total runoff rates increase over former savanna

and forest areas that have been converted to summer crops, and grassland that has been converted to winter crops (Fig. 9). Lower fall ET rates from summer crops (Fig. 8) lead to increases in winter total runoff. The largest changes ($\sim 0.6 \text{ mm day}^{-1}$; 45%) are found along the lower Mississippi. Fall ET rates over winter crops are actually greater than those of grasslands, but the large decreases in ET in summer allow soil moisture increases to remain through fall and contribute to increased winter total runoff rates. Summer crop ET rates over former northern grasslands increase during the crop-growing season so soil water is depleted and winter total runoff is decreased (see Fig. 4f).

In spring the pattern of decreased total runoff in the former northern grasslands has grown stronger ($\sim 0.2 \text{ mm day}^{-1}$; 20%) as more soil water is lost through evaporation from the bare summer crop fields (Fig. 4f). Total runoff also decreases over the winter wheat fields as the crops transpire at greater rates than grasses. Relatively large increases in total runoff are found in Indiana ($\sim 0.2 \text{ mm day}^{-1}$; 15%), where forest has been converted to summer crops and the lower crop transpiration rates compared to trees cause more water to be lost to drainage through the soil column (Fig. 3f).

Areas of significant increase in summer total runoff coincide with areas of decreased spring and summer ET rates over former savanna and forest ($\sim 0.2 \text{ mm day}^{-1}$; 35%), but the largest changes in summer total runoff correspond to the continued decrease over former northern grasslands ($\sim 0.4 \text{ mm day}^{-1}$; 25%). Much more water is evaporated in spring and transpired in summer from summer crop fields than the former grasslands, so there is less water available to drain through the soil column.

Like the annual average values of ET (Fig. 8), annual average total runoff values show few areas of statistically significant change. As expected, areas of increased ET show decreased total runoff. These decreases ($\sim 0.15 \text{ mm day}^{-1}$; 55 mm yr^{-1} or 75%) are found over former grasslands, particularly over former grasslands that are now planted as summer crops. Negligible changes are found over areas where spring crops are planted. Similarly, areas of decreased ET rates show increased total runoff rates. These areas are found over former grassland that has been converted to winter crops and over former savanna and forest ($\sim 0.25 \text{ mm day}^{-1}$; 91 mm yr^{-1} or 20%) that have been converted to summer crops.

6. Summary and conclusions

We used a land surface/ecosystem model, adapted for use over the continental United States, to investigate changes in the energy and water balance after land cover change in the Mississippi River basin. We first examined the physical processes involved in land cover change by running IBIS over a single 0.5° grid cell. We then used these results to help explain energy and water bal-

ance changes across the basin after a simulation of land cover change from a potential vegetation cover to a spatially explicit current land cover based on satellite and county-level survey data of crop cover.

Simulated changes in net radiation are driven mainly by changes in albedo. In general, net radiation decreases with forest conversion to crop cover and increases with grassland conversion to crop cover. Increases in net radiation during fall, winter, and spring after conversion of savanna to crops show that grasses dominate the savanna signal during those seasons, while decreases during summer suggest that the large LAI of trees in the savanna biome outweighs any effect of the grasses in this season.

Decreases in average annual LAI with forest conversion to cropland lead to decreases in simulated ET rates during all seasons, particularly in summer, even though the length of the evaporative season does not change. The decrease in transpiration over former forests in spring is compensated to some extent by soil evaporation from the bare crop fields but crop total runoff rates increase in all seasons after conversion. Even though there is a negligible change in average annual green LAI with a conversion from grasslands to spring and summer crops and a significant decrease with a conversion to winter crops, annual average ET and the length of the evaporative season increase after conversion as the lack of dormant grass cover in spring allows evaporation from bare crop fields. There is a decrease in spring total runoff for all crop types after conversion, while fall total runoff changes depend on crop type. Fall total runoff is less over summer crops as the growing season forces water loss through transpiration, there is no change in spring crop rates, and winter crop rates are greater as their early harvest leaves the entire summer for soil infiltration of water. The changes in water balance after conversion from savanna to summer crop cover are such that the trees of the potential savanna dominate any effects from the grasses.

Our simulation results suggest that total runoff has increased with a conversion from forest to current cover over the Mississippi River basin. Forests are found mainly in the eastern, humid, part of the basin. The more water-sensitive regions of the basin are found in the western, drier parts of the basin where a conversion from grasslands to current cover may decrease total runoff in the absence of irrigation and other human influences on the water budget. Even more important than annual changes may be the seasonal changes in water balance that are crop dependent. Much of the recharge to aquifers within the Mississippi River basin depends on snowmelt, so any changes in spring total runoff rates may be especially important to water resources. Our simulation has shown that the largest decreases in spring total runoff come from a grassland conversion to summer crops.

An assessment of the validity of the results from this kind of experiment is difficult given the lack of obser-

vations of energy and water balance changes after land cover change at the continental scale. Continuing improvements in technology of the remote sensing of surface characteristics and energy and water balance estimation may be useful for the validation of global- and regional-scale models such as IBIS. VanShaar et al. (2002) compared the sensitivity of two models to a simulated change in LAI over four catchments within the Columbia River basin and found that differences in the structures of the models made a noticeable difference in the change in water balance terms with land cover change. While IBIS-simulated energy, water, and crop-related (e.g., crop yield) terms have compared favorably to point observations over a variety of vegetation types and geographic locations (Foley et al. 1996; Costa and Foley 1997; Delire and Foley 1999; Lenters et al. 2000; Kucharik et al. 2001; Kucharik 2003), similar land cover change studies with different models should be performed to strengthen the confidence in the complex responses of biophysical and hydrological processes to land use and land cover change illustrated here.

Acknowledgments. This research was funded through the NASA Land Surface Hydrology Program and the University of Wisconsin—Madison Graduate School. The authors thank Michael Coe and Simon Donner for their help in directing the study and for their modeling expertise. The authors also thank the three reviewers whose contributions improved the manuscript.

REFERENCES

- Ball, J. T., I. E. Woodrow, and J. A. Berry, 1987: A model predicting stomatal conductance and its contribution to the control of photosynthesis under different environmental conditions. *Progress in Photosynthesis Research*, J. Biggins, Ed., Vol. 4, Martinus Nijhoff, 221–224.
- Baron, J. S., M. D. Hartman, T. G. F. Kittel, L. E. Band, D. S. Ojima, and R. B. Lammers, 1998: Effects of land cover, water redistribution, and temperature on ecosystem processes in the South Platte Basin. *Ecol. Appl.*, **8**, 1037–1051.
- Betts, R. A., 2001: Biogeophysical impacts of land use on present-day climate: Near-surface temperature change and radiative forcing. *Atmos. Sci. Lett.*, **2**, 39–51.
- Bonan, G. B., 1997: Effects of land use on the climate of the United States. *Climatic Change*, **37**, 449–486.
- , 1999: Frost followed the plow: Impacts of deforestation on the climate of the United States. *Ecol. Appl.*, **9**, 1305–1315.
- Bosch, J. M., and J. D. Hewlett, 1982: A review of catchment experiments to determine the effect of vegetation changes on water yield and evapo-transpiration. *J. Hydrol.*, **55**, 3–23.
- Botta, A., N. Viovy, P. Ciais, P. Friedlingstein, and P. Monfray, 2000: A global prognostic scheme of leaf onset using satellite data. *Global Change Biol.*, **6**, 709–725.
- Campbell, G. S., and J. M. Norman, 1998: *An Introduction to Environmental Biophysics*. Springer-Verlag, 286 pp.
- Chase, T. N., R. A. Pielke, T. G. F. Kittel, R. R. Nemani, and S. W. Running, 1996: Sensitivity of a general circulation model to global changes in leaf area index. *J. Geophys. Res.*, **101** (D3), 7393–7408.
- Coe, M. T., M. H. Costa, A. Botta, and C. Birkett, 2002: Long-term simulations of discharge and floods in the Amazon basin. *J. Geophys. Res.*, **107**, 8044, doi:10.1029/2001JD000740.
- Copeland, J. H., R. A. Pielke, and T. G. F. Kittel, 1996: Potential climatic impacts of vegetation change: A regional modeling study. *J. Geophys. Res.*, **101** (D3), 7409–7418.
- Costa, M. H., and J. A. Foley, 1997: Water balance of the Amazon basin: Dependence on vegetation cover and canopy conductance. *J. Geophys. Res.*, **102** (D20), 23 973–23 989.
- Delire, C., and J. A. Foley, 1999: Evaluating the performance of a land surface/ecosystem model with biophysical measurements from contrasting environments. *J. Geophys. Res.*, **104** (D14), 16 895–16 909.
- Dickinson, R. E., and A. Henderson-Sellers, 1988: Modelling tropical deforestation: A study of GCM land-surface parametrizations. *Quart. J. Roy. Meteor. Soc.*, **114**, 439–462.
- Donner, S. D., 2003: The impact of cropland cover on river nutrient levels in the Mississippi River basin. *Global Ecol. Biogeogr.*, **12**, 341–355.
- , and C. J. Kucharik, 2003: Evaluating the impacts of land management and climate variability on crop production and nitrate export across the upper Mississippi basin. *Global Biogeochem. Cycles*, **17**, 1085, doi:10.1029/2001GB001808.
- , M. T. Coe, J. D. Lenters, T. E. Twine, and J. A. Foley, 2002: Modeling the impact of hydrological changes on nitrate transport in the Mississippi River basin from 1955 to 1994. *Global Biogeochem. Cycles*, **16**, 1043, doi:10.1029/2001GB001396.
- Farquhar, G. D., and T. D. Sharkey, 1982: Stomatal conductance and photosynthesis. *Annu. Rev. Plant Physiol.*, **33**, 317–345.
- , S. von Caemmerer, and J. A. Berry, 1980: A biogeochemical model of photosynthetic CO₂ assimilation in leaves of C3 species. *Planta*, **149**, 78–90.
- Foley, J. A., A. Botta, and M. T. Coe, 2002: El Niño–Southern oscillation and the climate, ecosystems and rivers of Amazonia. *Global Biogeochem. Cycles*, **16**, 1132, doi:10.1029/2002GB001872.
- , I. C. Prentice, N. Ramankutty, S. Levis, D. Pollard, S. Sitch, and A. Haxeltine, 1996: An integrated biosphere model of land surface processes, terrestrial carbon balance, and vegetation dynamics. *Global Biogeochem. Cycles*, **10**, 603–628.
- Geng, S., F. W. T. Penning De Vries, and I. Supit, 1985: A simple method for generating daily rainfall data. *Agric. For. Meteorol.*, **36**, 363–376.
- Hansen, J. E., 1998: Climate forcings in the Industrial Era. *Proc. Natl. Acad. Sci.*, **95**, 12 753–12 758.
- Jones, C. A., and J. R. Kiniry, Eds., 1986: *CERES-Maize: A Simulation Model of Maize Growth and Development*. Texas A&M University Press, 194 pp.
- Kalnay, E., and Coauthors, 1996: The NCEP/NCAR 40-Year Reanalysis Project. *Bull. Amer. Meteor. Soc.*, **77**, 437–471.
- Kucharik, C. J., 2003: Evaluation of a process-based agro-ecosystem model (Agro-IBIS) across the U.S. cornbelt: Simulations of the interannual variability in maize yield. *Earth Interactions*, **7**. [Available online at <http://EarthInteractions.org>.]
- , and K. R. Brye, 2003: Integrated Biosphere Simulator (IBIS) yield and nitrate loss predictions for Wisconsin maize receiving varied amounts of Nitrogen fertilizer. *J. Environ. Qual.*, **32**, 247–268.
- , and Coauthors, 2000: Testing the performance of a dynamic global ecosystem model: Water balance, carbon balance, and vegetation structure. *Global Biogeochem. Cycles*, **14**, 795–825.
- , K. R. Brye, J. M. Norman, J. A. Foley, S. T. Gower, and L. G. Bundy, 2001: Measurements and modeling of carbon and nitrogen cycling in agroecosystems of southern Wisconsin: Potential for SOC sequestration during the next 50 years. *Ecosystems*, **4**, 237–258.
- Lenters, J. D., M. T. Coe, and J. A. Foley, 2000: Surface water balance of the continental United States, 1963–1995: Regional evaluation of a terrestrial biosphere model and the NCEP/NCAR reanalysis. *J. Geophys. Res.*, **105** (D17), 22 393–22 425.
- Loveland, T. R., and A. S. Belward, 1997: The IGBP-DIS global 1 km land cover data set, DISCover. *Int. J. Remote Sens.*, **18**, 3289–3295.

- Matheussen, B., R. L. Kirschbaum, I. A. Goodman, G. M. O'Donnell, and D. P. Lettenmaier, 2000: Effects of land cover change on streamflow in the interior Columbia River basin (USA and Canada). *Hydrol. Processes*, **14**, 867–885.
- Miller, D. A., and R. A. White, 1998: A conterminous United States multi-layer soil characteristics data set for regional climate and hydrology modeling. *Earth Interactions*, **2**. [Available online at <http://EarthInteractions.org>.]
- Myrhe, G., and A. Myrhe, 2003: Uncertainties in radiative forcing due to surface albedo changes caused by land-use changes. *J. Climate*, **16**, 1511–1524.
- New, M., M. Hulme, and P. D. Jones, 1999: Representing twentieth century space–time climate variability. Part I: Development of a 1961–90 mean monthly terrestrial climatology. *J. Climate*, **12**, 829–856.
- Pielke, R. A., R. L. Walko, L. T. Steyaert, P. L. Vidale, G. E. Liston, W. A. Lyons, and T. N. Chase, 1999: The influence of anthropogenic landscape changes on weather in south Florida. *Mon. Wea. Rev.*, **127**, 1663–1673.
- Ramankutty, N., and J. A. Foley, 1998: Characterizing patterns of global land use: An analysis of global croplands data. *Global Biogeochem. Cycles*, **12**, 667–685.
- , and —, 1999: Estimating historical changes in land cover: North American crops from 1850 to 1992. *Global Ecol. Biogeogr.*, **8**, 381–396.
- Rawls, W. J., L. R. Ahuja, and D. L. Brakensiek, 1992: Estimating soil hydraulic properties from soils data. *Indirect Methods for Estimating Hydraulic Properties of Unsaturated Soils*, M. th. Van Genuchten, F. J. Leij, and L. J. Lund, Eds., University of California Riverside Press, 718 pp.
- Richardson, C. W., 1981: Stochastic simulation of daily precipitation, temperature, and solar radiation. *Water Resour. Res.*, **17**, 182–190.
- , and D. A. Wright, 1984: WGEN: A model for generating daily weather variables. Agricultural Research Service Rep. ARS-8, U.S. Department of Agriculture, 83 pp.
- Sharpley, A. N., and J. R. Williams, 1990: EPIC—Erosion/Productivity Impact Calculator: 1. Model documentation. Tech. Bull. 1768, U.S. Department of Agriculture, 235 pp.
- Thompson, S. L., and D. Pollard, 1995a: A global climate model (GENESIS) with a land-surface transfer scheme (LSX). Part I: Present climate simulation. *J. Climate*, **8**, 732–761.
- , and —, 1995b: A global climate model (GENESIS) with a land-surface-transfer scheme (LSX). Part II: CO₂ sensitivity. *J. Climate*, **8**, 1104–1121.
- VanShaar, J. R., I. Haddeland, and D. P. Lettenmaier, 2002: Effects of land-cover changes on the hydrological response of interior Columbia River basin forested catchments. *Hydrol. Processes*, **16**, 2499–2520.
- Vorosmarty, C. J., and B. Moore, 1991: Modeling basin-scale hydrology in support of physical climate and global biogeochemical studies: An example using the Zambezi River. *Surv. Geophys.*, **12**, 271–311.
- , —, A. L. Grace, M. P. Gildea, J. M. Melillo, B. J. Peterson, E. B. Rastetter, and P. A. Steudler, 1989: Continental scale models of water balance and fluvial transport: An application to South America. *Global Biogeochem. Cycles*, **3**, 241–265.
- White, M. A., P. E. Thornton, and S. W. Running, 1997: A continental phenology model for monitoring vegetation responses to inter-annual climatic variability. *Global Biogeochem. Cycles*, **11**, 217–234.